

Article

# Coulomb-Nuclear Interference in polarized pA scattering

Boris Kopeliovich <sup>1,\*</sup>, Michal Krelina <sup>2</sup>, Irina Potashnikova <sup>1</sup>

<sup>1</sup> Universidad Técnica Federico Santa María, Avenida España 1680, Valparaíso, Chile

<sup>2</sup> Czech Technical University in Prague, FNSPE, Břehová 7, 11519 Prague, Czech Republic

\* Correspondence: boris.kopeliovich@usm.cl

**Abstract:** We made the first attempt to understand the observed unusual t-dependence of single-spin asymmetry observed in the HJET experiment at RHIC. On the contrary to the usual division of the interaction amplitudes to pure electromagnetic and strong interaction terms with Coulomb corrections (Coulomb phase), we combine Usually the interaction of hadrons is presented as long-range Coulomb interaction and short-range strong interaction with Coulomb corrections. Such a division gives rise to a Coulomb phase of the hadronic term. On the contrary, here we consider short-range hadronic interaction as a correction to the long-range electromagnetic term, i.e. treat it as absorptive corrections. They significantly affect the Coulomb-nuclear interference, which is a source of single-spin azimuthal asymmetry at very small angles.

**Keywords:** single spin asymmetry, Coulomb nuclear interference, Pomeron spin

## 1. Introduction

Azimuthal asymmetry  $A_N$  in polarized elastic hadronic scattering comes from interference of the spin-flip  $f_{sf}$  and non-flip  $f_{nf}$  amplitudes. The differential elastic cross sections and single-spin asymmetry  $A_N(t)$ , where  $t$  is 4-momentum transfer squared, are expressed via these amplitudes as,

$$\frac{d\sigma_{el}}{dt} = \pi(|f_{nf}|^2 + |f_{sf}|^2), \quad (1)$$

$$A_N \frac{d\sigma_{el}}{dt} = -2\pi \text{Im}(f_{nf} f_{sf}^*). \quad (2)$$

This is why polarization effects are usually considered as a sensitive tool for study of the hadron interaction dynamics [1,2].

In the Regge-pole model the pure hadronic asymmetry Eq. (2) vanishes because  $f_{sf}^h$  and  $f_{sf}^h$  have the same phase given by the signature factor. To maximize  $A_N(t)$  one should combine hadronic and electromagnetic amplitudes [3]. While the former is predominantly imaginary, the latter is nearly real. Apparently, a sizable effect is expected at small momentum transfer squared  $t$ , where the Coulomb and hadronic amplitudes are of the same order. The  $t$  dependence of asymmetry in  $pp$  scattering is described in a simplified approximation [3] by,

$$A_N^{pp}(t) = A_N^{pp}(t_p) \frac{4y^{3/2}}{3y^2 + 1}, \quad (3)$$

where  $y = -t/t_p^{pp}$  and

$$t_p^{pp} = \frac{8\sqrt{3}\pi\alpha_{em}}{\sigma_{tot}^{pp}}; \quad (4)$$

$$A_N^{pp}(t_p) = \frac{\sqrt{3}t_p}{4m_p} (\mu_p - 1). \quad (5)$$

arXiv:2312.03702v1 [hep-ph] 6 Dec 2023



**Citation:** Kopeliovich, Krelina, Potashnikova Coulomb-Nuclear Interference in polarized pA scattering. *Universe* **2023**, *1*, 0. <https://doi.org/>

Received:  
Accepted:  
Published:



**Copyright:** © 2023 by the authors. Licensee MDPI, Basel, Switzerland. This article is an open access article distributed under the terms and conditions of the Creative Commons Attribution (CC BY) license (<https://creativecommons.org/licenses/by/4.0/>).

Here  $\alpha_{em} = 1/137$  is the fine structure constant;  $\mu_p = 2.79$  is the proton magnetic moment. The asymmetry  $A_N^{pp}(t)$  reaches a maximum (5) of about 4-5%, at  $t = t_p \approx 2 \times 10^{-3} \text{ GeV}^2$ . For the sake of simplicity we assume here, like in [3], a pure non-flip and imaginary hadronic amplitude, no Coulomb phase, etc. In what follows, we give up most of these simplifications. The predicted in [3] CNI asymmetry Eq. (3) was well confirmed by the first [4] and following [5] measurements in  $pp$  collisions.

Similar relations can be applied to proton-nucleus elastic scattering with apparent modifications

$$t_p^{pA} = K_A t_p^{pp}, \tag{6}$$

with

$$K_A = \frac{Z\sigma_{tot}^{pp}}{\sigma_{tot}^{pA}}. \tag{7}$$

Correspondingly, the maximal value of  $A_N$  at  $t = t_p^{pA}$  reads,

$$A_N^{pA}(t_p^{pA}) = \sqrt{K_A} A_N^{pp}(t_p). \tag{8}$$

A simple estimate  $\sigma_{tot}^{pA} \sim A^{2/3}\sigma_{tot}^{pp}$  leads to non-dramatic modification of the CNI asymmetry, about 20% increase of  $A_N^{pA}(t_p^{pA})$  even for heavy nuclei, e.g. gold.

Important is nuclear suppressed spin-flip amplitude related to the Pomeron. The energy of 100 GeV in the Lab frame is not sufficiently high to suppress iso-vector Reggeons, which have quite a large (dominating) spin-flip component. This is why it is difficult to disentangle large Reggeon and small Pomeron spin-flip terms. On iso-scalar nuclei, e.g. carbon, copper, etc. iso-vector Reggeons are completely excluded, otherwise are suppressed by a small factor  $(A - 2Z)/A$ .

### 2. Born approximation

The elastic  $pA$  amplitude is fully described by two helicity amplitudes  $f_{nf, sf}$  defined in [2], each having hadronic and electromagnetic parts,  $f_i(q_T) = f_i^h(q_T) + f_i^{em}(q_T)$ , where for small-angle elastic scattering  $t \equiv -q^2 \approx -q_T^2$

Hadronic Born amplitudes can be represented as

$$f_{nf}^{pA(h)}(q_T)|_B = \frac{\sigma_{tot}^{pA}}{4\pi} F_A^h(q_T^2), \tag{9}$$

$$f_{sf}^{pA(h)}(q_T)|_B = r_5^{pA} \frac{q_T}{m_N} \frac{\sigma_{tot}^{pA}}{4\pi} \text{Im} F_A^h(q_T^2), \tag{10}$$

where  $r_5^{pA}$  is a nuclear analog of  $r_5^{pp}$  defined in [2]

$$r_5 = \frac{m_N f_{sf}(q_T)}{q_T \Im f_{nf}(q_T)} \tag{11}$$

For  $pp$  elastics scattering it was fitted to data in [5,6].

The hadronic nuclear formfactors  $F_A^h(q_T^2)$  in Eqs. (9)-(10) also can be evaluated within the Glauber approximation [7])

$$F_A^h(q_T) = \frac{2i}{\sigma_{tot}^{pA}} \int d^2b e^{i\vec{q}_T \cdot \vec{b}} \left[ 1 - \left( 1 - \frac{1}{2A} \sigma_{tot}^{pp} (1 - i\rho_{pp}(s)) T_A^h(b) \right)^A \right], \tag{12}$$

as well as the total nuclear cross section,

$$\sigma_{tot}^{pA} = 2\text{Im} \int d^2b i \left[ 1 - \left( 1 - \frac{1}{2A} \sigma_{tot}^{pp}(s) (1 - i\rho_{pp}(s)) T_A^h(b) \right)^A \right]. \tag{13}$$

Correspondingly, the Born electromagnetic amplitudes read,

$$f_{nf}^{pA(em)}(q_T) \Big|_B = -2Z\alpha_{em} \frac{1}{q_T^2 + \lambda^2} F_A^{em}(q_T), \tag{14}$$

$$f_{sf}^{pA(em)}(q_T) \Big|_B = -Z\alpha_{em} \frac{1}{m_N q_T} (\mu_p - 1) F_A^{em}(q_T), \tag{15}$$

where a small fictitious photon mass  $\lambda$  is introduced to avoid infra-red divergence. The final results will be checked for stability at  $\lambda \rightarrow 0$ .

Nuclear electromagnetic formfactor in in Eqs. (14)-(23B) have the form,

$$F_A^{em}(q_T) = \frac{1}{Z} \int d^2b e^{i\vec{q}_T \cdot \vec{b}} T_Z(b), \tag{16}$$

The nuclear thickness functions are defined as,

$$T_A(b) = \int_{-\infty}^{\infty} dz \rho(b, z), \tag{17}$$

where  $\rho(b, z)$  is the nuclear density distribution function, and  $T_Z(b) = T_A(b) Z / A$ .

Following [7,8] in what follows we replace the nuclear thickness function by a more accurate effective thickness function convoluted with NN elastic amplitude

$$T_A(b) \Rightarrow T_A^h(b), \tag{18}$$

where

$$T_A^h(b) = \frac{2}{\sigma_{tot}^{hN}} \int d^2s \text{Re}\Gamma^{hN}(s) T_A(\vec{b} - \vec{s}); \tag{19}$$

$$\text{Re}\Gamma^{hN}(s) = \frac{\sigma_{tot}^{hN}}{4\pi B_{hN}} \exp\left(-\frac{s^2}{2B_{hN}}\right), \tag{20}$$

where  $B_{hN}$  is the slope of the differential  $hN$  elastic cross section. This effective nuclear thickness function can be simplified to

$$\begin{aligned} T_A^h(b) &= \frac{2}{\sigma_{tot}^{hN}} \int d^2s \frac{\sigma_{tot}^{hN}}{4\pi B_{hN}} \exp\left(-\frac{s^2}{2B_{hN}}\right) T_A(\vec{b} - \vec{s}) \\ &= \frac{1}{2\pi B_{hN}} \int ds d\phi s \exp\left(-\frac{s^2}{2B_{hN}}\right) T_A(\sqrt{b^2 + s^2 - 2bs \cos \phi}). \end{aligned} \tag{21}$$

### 3. Hadronic vs electromagnetic amplitudes

The long-range Coulomb forces also affect the strong-interaction amplitude. This is illustrated in Fig. 1, following the consideration of this problem in [9]. These graphs can be grouped and interpreted differently. One way, employed in [9], is to combine the last two graphs, (N) and (CN), and treat it as a Coulomb modified strong-interaction amplitude. The modification is approximated by giving an extra phase factor to the hadronic amplitude. This factor is called in the literature Coulomb phase [9–11].

Otherwise, one can combine (C) with (CN) and get a hadronic correction to the Coulomb amplitude. In what follows we call this absorptive correction [12,13].

As usual, multiple interaction amplitudes, depicted in Fig. 1 are easily calculated in impact parameter representation, where the result is just a product of multiple amplitudes.

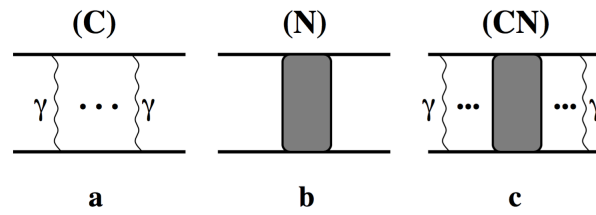


**Figure 1.** Three types of interaction: pure electromagnetic (a), pure strong interaction (b), and combined strong an electromagnetic interactions (c).

So we switch from  $q_T$  to  $b$  dependent amplitudes, and simultaneously from the Born approximation to the eikonal optical model.

$$\gamma_{nf}^{pA(h)}(b) = \frac{i}{2\pi} \int d^2q_T e^{-i\vec{q}_T \cdot \vec{b}} f_{nf}^{pA(h)}(q_T) \tag{22}$$

$$\gamma_{sf}^{pA(h)}(b) = \frac{i}{2\pi} \int d^2q_T e^{-i\vec{q}_T \cdot \vec{b}} f_{sf}^{pA(h)}(q_T) \tag{23}$$

These hadronic eikonal phase was used in the Glauber model expressions (12), (13).

Adding higher order terms to the Born Coulomb amplitudes (22)-(23) we arrive at the eikonal form for the electromagnetic amplitudes, as well,

$$f_{nf}^C(q_T) = \frac{i}{2\pi} \int d^2b e^{i\vec{q}_T \cdot \vec{b}} \left( 1 - e^{i\chi_{nf}^C(b)} \right), \tag{24}$$

$$f_{sf}^C(q_T) = \frac{1}{2\pi} \int d^2b e^{i\vec{q}_T \cdot \vec{b}} \chi_C^{sf}(b) e^{i\chi_{nf}^C(b)}, \tag{25}$$

with Coulomb eikonal phases,

$$\chi_{nf}^C(b) = \frac{-2Z\alpha_{em}}{2\pi} \int d^2q_T e^{-i\vec{q}_T \cdot \vec{b}} \frac{F_A^{em}(q_T)}{q_T^2 + \lambda^2} \tag{26}$$

$$\chi_{sf}^C(b) = \frac{-Z\alpha_{em}(\mu_p - 1)}{2\pi m_N} \int d^2q_T e^{-i\vec{q}_T \cdot \vec{b}} \frac{F_A^{em}(q_T)}{q_T^2 + \lambda^2} \frac{\vec{q}_T \cdot \vec{b}}{b}. \tag{27}$$

Combining the Coulomb (C) with Coulomb-nuclear (CN) mechanisms depicted in Fig. 1, one gets the Coulomb terms, Eqs. (24) or (25), which acquire an absorption factor,

$$S(b) = 1 - \gamma_{nf}^{pA(h)}(b) = \left( 1 - \frac{1}{2A} \sigma_{tot}^{pp}(s) (1 - i\rho_{pp}(s)) T_A^h(b) \right)^A \approx \exp \left[ -\frac{1}{2} \sigma_{tot}^{pp}(s) T_A^h(b) \right] \tag{28}$$

Thus, the absorption corrected amplitudes  $\tilde{f}$  take the form,

$$\tilde{f}_{nf}^C(q_T) = \frac{i}{2\pi} \int d^2b e^{i\vec{q}_T \cdot \vec{b}} \left( 1 - e^{i\chi_{nf}^C(b)} \right) S(b), \tag{29}$$

$$\tilde{f}_{sf}^C(q_T) = \frac{1}{2\pi} \int d^2b e^{i\vec{q}_T \cdot \vec{b}} \chi_C^{sf}(b) e^{i\chi_{nf}^C(b)} S(b), \tag{30}$$

Eventually, we arrived at the full amplitudes.

$$f_{nf,sf}(q_T) = \tilde{f}_{nf,sf}^C(q_T) + f_{nf,sf}^N(q_T). \tag{31}$$

#### 4. Results vs data

Now we are in a position to calculate the proton-nucleus total cross section and single-spin asymmetry, given by Eqs. (1)-(2). The results are compared with data in Figs. 2 - 5.

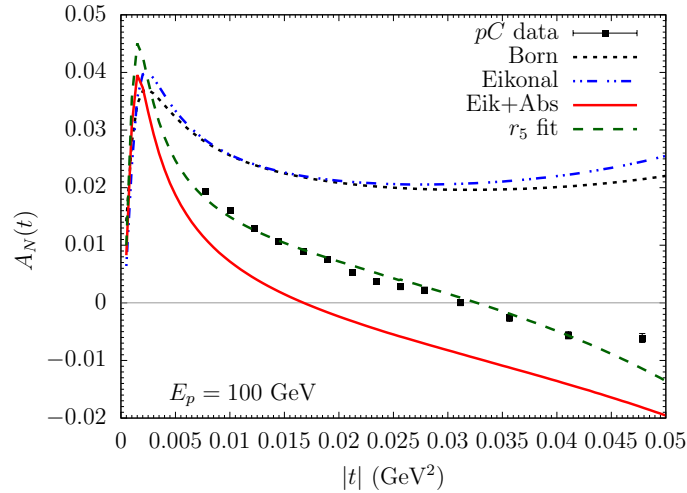


**Figure 2.** Azimuthal asymmetry in proton-Carbon elastic scattering. Black dotted curve presents Born approximation, Eqs. (9)-(10) and (14)-(15). Double-dot-dashed blue and solid red curves, correspond to Eikonal approximation without, (24)-(25), and with (29)-(30), absorptive corrections, respectively. In both cases  $r_5^{pA} = 0$ ; Data for  $pC$  scattering at 100 GeV are from [14]

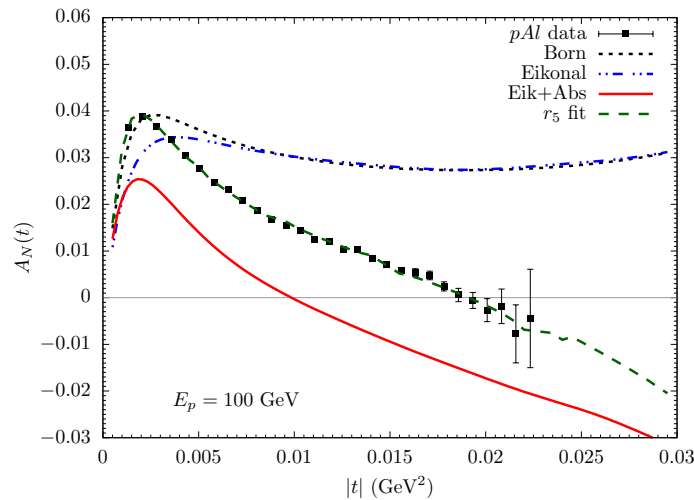


**Figure 3.** The same as in Fig. 2, but for proton-Aluminium elastic scattering. Data at 100 GeV are from [15]

First of all we performed calculations within the Born approximation, Eqs. (9)-(10) and (14)-(15). The hadronic spin-flip component was set to zero. The results are depicted with black dotted curves in Figs. 2 - 5. The magnitude of  $A_N$  substantially exceeds data.

Then we relied on the eikonal form of higher order terms, Eqs. (24)-(25) keeping  $r_5 = 0$ . The results are depicted with blue double-dot-dashed curves. The effect of eikonalization turns out to be rather mild, the discrepancy with data remains significant.

The next step is introduction of absorptive corrections, which significantly reduce the values of  $A_N(t)$  as is demonstrated by red solid curves, calculated with Eqs. (29)-(30) ( $r_5$  is still zero).

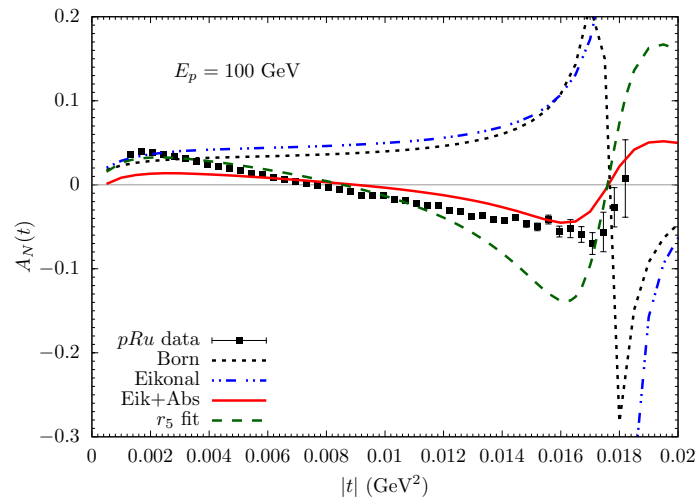


**Figure 4.** The same as in Fig. 2, but for proton-Ruthenium elastic scattering. Data at 100 GeV are from [16]

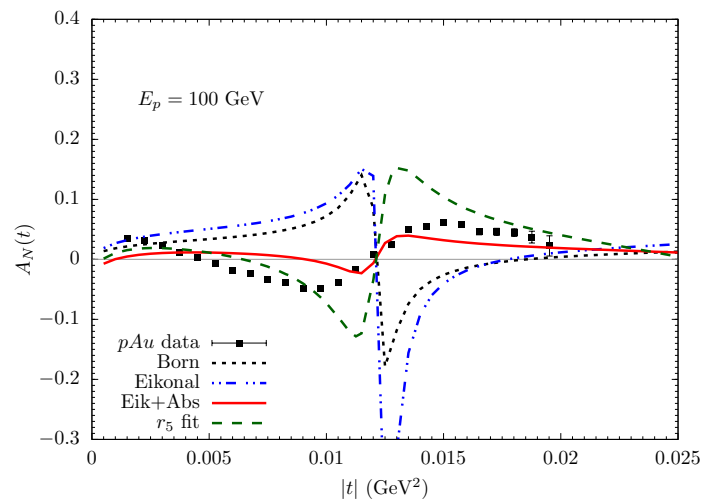


**Figure 5.** The same as in Fig. 2, but for proton-Gold elastic scattering. Data at 100 GeV are from [15,16]

Eventually, we can adjust the single unknown parameter,  $r_5^{pA}$  for each nuclear target. The results of the fit are presented in Table 1. The found values of  $r_5^{pA}$  are pretty close to

Experiment	Re $r_5$ fit	Im $r_5$ fit
p-C @ 100 GeV	$-0.071 \pm 0.003$	$-0.063 \pm 0.005$
p-Al @ 100 GeV	$-0.080 \pm 0.001$	$-0.101 \pm 0.002$
p-Ru @ 100 GeV	$-0.068 \pm 0.001$	$-0.469 \pm 0.002$
p-Au @ 100 GeV	$-0.027 \pm 0.008$	$-0.526 \pm 0.006$

**Table 1.** Results of fit for  $r_5^{pA}$  to data on  $A_N(t)$  for different nuclei [14–16].

the values for the Pomeron spin component found by fit to  $pp$  data in [6].

With values of  $r_5$  in Table 1 and amplitudes Eqs. (29)–(30) we plot the green dashed curves, which we treat as our final results.

Notice that nuclear data are quite sensitive to the value of  $r_5^{pA}$ , this is why the CNI method was proposed [17] as a unique way for measuring the hadronic spin-flip amplitudes at high energies.

## 5. Conclusions

Concluding, we performed the first calculation of single-spin asymmetry in polarized proton-nucleus elastic scattering in the CNI region. We achieved a reasonable agreement with data, in spite of rather complicated theoretical construction. The remarkable feature of the nuclear formfactor (12) is a change of sign of the imaginary part of elastic hadronic non-flip amplitude corresponding to the first zero of the Bessel function  $J_1(t)$ . Since the non-flip hadronic amplitude significantly exceeds the spin-flip part they become of the same order right before and after the former changes sign. The asymmetry  $A_N(t)$  Eq. (2) reaches maximum at  $f_{nf} = f_{sf}$ , so  $A_N(t)$  should abruptly vary between positive and negative maxima in the vicinity of the Bessel zero. Comparison with data in Figs. 4–5 confirms such a behavior, indeed the measured  $A_N(t)$  exposes two maxima with opposite signs with positions close to predicted.

However the magnitude of these maxima is exaggerate in our calculations, so there is still room for improvements. Here nuclear effects were evaluated within the Glauber approximation, which is subject to Gribov inelastic shadowing corrections [18,19]. Their calculation require a subsantial modelling, including knowledge of the proton wave function, interaction mechanism, etc. This need a detailed study, like it was done in [8]. We leave this issue for future developments.

**Acknowledgments:** This work was supported in part by grants ANID - Chile FONDECYT 1231062, by ANID PIA/APOYO AFB220004, and by ANID - Millennium Science Initiative Program ICN2019\_044.

1. S. M. Bilenky, L. I. Lapidus and R. M. Ryndin, “Polarized proton target in experiments with high-energy particles,” *Sov. Phys. Usp.* **7** (1965) 721 [*Usp. Fiz. Nauk* **84** (1964) 243].
2. N. H. Buttimore, B. Z. Kopeliovich, E. Leader, J. Soffer and T. L. Trueman, “The spin dependence of high-energy proton scattering,” *Phys. Rev. D* **59** (1999) 114010.
3. B. Z. Kopeliovich and L. I. Lapidus, “On the necessity of polarization experiments in colliding p and anti-p beams,” *Yad. Fiz.* **19** (1974) 218.
4. N. Akchurin *et al.* [E581/704 Collaboration], “Analyzing power measurement of p p elastic scattering in the Coulomb - nuclear interference region with the 200-GeV/c polarized proton beam at Fermilab,” *Phys. Rev. D* **48** (1993) 3026.
5. A. A. Poblaguev *et al.*, “Precision Small Scattering Angle Measurements of Elastic Proton-Proton Single and Double Spin Analyzing Powers at the RHIC Hydrogen Jet Polarimeter,” *Phys. Rev. Lett.* **123** (2019) 162001.
6. B. Z. Kopeliovich, M. Krelina and I. K. Potashnikova, “Probing the Pomeron spin structure with Coulomb-nuclear interference,” *Phys. Lett. B* **816** (2021), 136262.

7. B. Z. Kopeliovich, "Transparent nuclei and deuteron gold collisions at RHIC," *Phys. Rev. C* **68** (2003), 044906.
8. B. Z. Kopeliovich, I. K. Potashnikova and I. Schmidt, "Large rapidity gap processes in proton-nucleus collisions," *Phys. Rev. C* **73** (2006), 034901.
9. B. Z. Kopeliovich and A. V. Tarasov, "The Coulomb phase revisited," *Phys. Lett. B* **497** (2001), 44-48.
10. H.A. Bethe, "Scattering and polarization of protons by nuclei", *Ann. Phys.* **3** (1958) 190-240.
11. R.N. Cahn, "Coulombic-hadronic interference in an eikonal model", *Z. Phys. C* **15** (1982) 253-260.
12. B. Z. Kopeliovich, "High-energy polarimetry at RHIC," [arXiv:hep-ph/9801414 [hep-ph]].
13. B. Z. Kopeliovich and T. L. Trueman, "Polarized proton nucleus scattering," *Phys. Rev. D* **64** (2001) 034004.
14. O. Jinnouchi, I. G. Alekseev, A. Bravar, G. Bunce, S. Dhawan, H. Huang, G. Igo, V. P. Kanavets, K. Kurita and H. Okada, *et al.* "Measurement of the analyzing power of proton-carbon elastic scattering in the CNI region at RHIC," [arXiv:nucl-ex/0412053 [nucl-ex]].
15. A. Poblaguev, "New DAQ for the HJET polarimeter at RHIC," *PoS PSTP2015*, 032 (2015).
16. A. Poblaguev, "Precision small scattering angle measurements of proton-proton and proton-nucleus analyzing powers at the RHIC hydrogen jet polarimeter", *Acta Physica Polonica B Proceedings Supplement* **16** no. 5, (2023) 1.
17. B. Z. Kopeliovich and B. G. Zakharov, "Spin - Flip Component of the Pomeron," *Phys. Lett. B* **226**, 156 (1989).
18. V. N. Gribov, "Glauber Corrections And The Interaction Between High-Energy Hadrons And Nuclei," *Sov. Phys. JETP* **29**, 483 (1969) [*Zh. Eksp. Teor. Fiz.* **56**, 892 (1969)].
19. B. Z. Kopeliovich, "Gribov inelastic shadowing in the dipole representation," *Int. J. Mod. Phys. A* **31**, no.28n29, 1645021 (2016).